



HAL
open science

Coupling of clouds and tropospheric relative humidity in the tropical Western Atlantic: insights from multisatellite observations

Hélène Brogniez, Pierre-Emmanuel Kirstetter

► **To cite this version:**

Hélène Brogniez, Pierre-Emmanuel Kirstetter. Coupling of clouds and tropospheric relative humidity in the tropical Western Atlantic: insights from multisatellite observations. *Geophysical Research Letters*, 2020, 47 (7), pp.e2020GL087466. 10.1029/2020GL087466 . insu-02514961

HAL Id: insu-02514961

<https://insu.hal.science/insu-02514961>

Submitted on 18 Nov 2020

HAL is a multi-disciplinary open access archive for the deposit and dissemination of scientific research documents, whether they are published or not. The documents may come from teaching and research institutions in France or abroad, or from public or private research centers.

L'archive ouverte pluridisciplinaire **HAL**, est destinée au dépôt et à la diffusion de documents scientifiques de niveau recherche, publiés ou non, émanant des établissements d'enseignement et de recherche français ou étrangers, des laboratoires publics ou privés.

1 **Coupling of clouds and tropospheric relative humidity**
2 **in the tropical Western Atlantic: insights from**
3 **multi-satellite observations**

4 **Hélène Brogniez¹, Pierre-Emmanuel Kirstetter²**

5 ¹LATMOS/IPSL, UVSQ Université Paris-Saclay, Sorbonne Université, CNRS, Guyancourt, France

6 ²University of Oklahoma / NOAA National Severe Storm Laboratory, Norman, USA

7 **Key Points:**

- 8 • The daytime drying of the mid-troposphere is associated with the large-scale subsi-
9 dence and presumably with the diurnal pulses of ITCZ.
- 10 • The diurnal cycle of upper-level cloudiness is essential for tropospheric moistening by
11 inducing local lifting.
- 12 • The upper level moisture feeds upper-level clouds and modulates their diurnal cycle.

Corresponding author: H. Brogniez, helene.brogniez@latmos.ipsl.fr

Abstract

We investigated the interactions between clouds and moisture at the diurnal scale in the Western Atlantic trade winds region. Profiles of tropospheric relative humidity from the SAPHIR/Megha-Tropiques sounder are combined with cloud categories obtained from geostationary satellites. In Winter, the mid-troposphere undergoes strong daytime drying due to air masses coming from the colder upper troposphere. The moistening near the surface triggered by solar radiation precludes the development of low-level clouds. At night rising moist air in the upper troposphere triggers the formation of high-altitude clouds and favors their presence. In Summer, daytime high-altitude clouds shield the solar forcing on the atmosphere and reduce drying from large-scale subsidence. After sunset, the development of upper tropospheric opaque clouds constitutes a local source of moisture. We argue that modulations of the diurnal cycle of clouds and relative humidity by season may be related to diurnal pulses of the ITCZ.

Plain Language Summary

The heat engine of the climate is the atmospheric water cycle. Understanding the relationships between clouds and the atmospheric relative humidity is crucial to improve our understanding of climate variability. Here we focus on the diurnal fluctuations of vertical profiles of tropospheric relative humidity and collocated clouds in the tropical Western Atlantic trade winds region. Profiles of water vapor and distribution of clouds, classified by altitudes, are obtained from space-borne instruments, and the other environmental characteristics such as sea surface and air temperatures are extracted from a weather model. Their joint diurnal variations are examined. Winter and Summer seasons are compared. The diurnal water vapor cycle of water vapor evolves from the bottom to the top of the atmosphere and is strongly associated with cloud types, with a seasonal modulation. During daytime a strong drying is associated with the downward dry air masses moving downward. The diurnal cycle of upper-level cloudiness plays a critical role in inhibiting daytime drying by shielding the mid-troposphere from this downward transport. The upper-level moisture feeds upper-level clouds and modulates their diurnal lifetime.

1 Introduction

There is no doubt that we need to improve our understanding of how clouds and cloud-related feedbacks impact on climate (Stephens et al., 2002; Bony et al., 2015). Critical

44 processes involving clouds and water vapor, such as detrainment and evaporation, typically
45 occur at time scales of less than 6 hours. This calls for sub-daily analyses of observations.
46 Regional variations in the diurnal cycle of clouds are caused by several parameters such
47 as orography, land/sea circulation, air-sea fluxes and sea surface temperature (SST), their
48 effect differing with the dominant cloud type (Yang & Slingo, 2001; Eastman & Warren,
49 2014; Noel et al., 2018). The role of the free tropospheric water vapor in the evolution of
50 clouds at the diurnal scale has not been extensively studied due to lack of observations. An
51 improved understanding of how different cloud types and their diurnal cycles interact with
52 the atmospheric water vapor is much needed in order to make the connections between the
53 solar forcing, the surface and the atmospheric water cycle (cloud, vapor and rain).

54 For example, observations of rainfall rates associated with deep convection in the Indian
55 Ocean warm pool region have revealed a predawn rainfall peak (Mapes & Houze, 1993;
56 Sakaeda et al., 2018) triggered by solar absorption (Sakazaki et al., 2017) and invigorated
57 by the oceanic warm layer in some regions (Bellenger et al., 2010). Ruppert and Johnson
58 (2015) have highlighted the existence of a deepening of daytime convective clouds along
59 with a parallel increase in moisture in the lower troposphere. In this region of the upward
60 branch of the ITCZ characterized by active convection, these diurnal pulses are favored
61 by a combination of increasing SST in the daytime and a reduced large-scale subsidence.
62 These pulses are thought to further affect remote shallow convective areas through a strong
63 feedback on daily precipitation and convective heating (Ruppert, 2016; Ciesielski et al.,
64 2018).

65 The impact of clouds on solar radiation and related heating has also been addressed
66 in numerous works. The direct absorption of shortwave radiation by optically opaque and
67 elevated clouds (anvil-type clouds) is thought to cause a strong cloud-top heating (Hartmann
68 et al., 1984; Ackerman et al., 1988; Mather et al., 2007; Powell et al., 2012) that increases
69 buoyancy below, and a lifting towards the upper-levels, thereby causing a daytime peak in
70 upper-level cloudiness to prevail (Ruppert & Klocke, 2019). Atmospheric tides, driven by
71 solar heating and ozone absorption, have also an effect in the diurnal convection cycle and
72 subsequent precipitation (Woolnough et al., 2004).

73 Studies focusing on oceanic shallow convective clouds, such as Stratocumulus and Cu-
74 mulus, have shown that their diurnal cycle is linked to lower-tropospheric stability with a
75 large-scale meteorological influence (Klein & Hartmann, 1993; Wood, 2012). The maximum

76 of occurrence of these low-level clouds has been observed in the early morning hours before
77 sunrise and their diurnal cycle depend strongly on the region (Klein et al., 1995; Rozendaal
78 et al., 1995; Eastman & Warren, 2014). The recent work of Vial et al. (2019) highlighted the
79 challenge for high resolution models to represent the daily cycle of such shallow clouds. For
80 example Chung et al. (2007) examined convectively active parts of Africa and the Atlantic
81 ocean with the METEOSAT geostationary satellite. They revealed a peak on the Upper
82 Tropospheric Humidity (UTH) at 3:00LT with a clear contrast between land and ocean,
83 which remains a challenge to represent in several reanalyzes, thereby highlighting missing
84 processes related to moisture (Chung et al., 2013).

85 To our knowledge, few studies have analyzed the diurnal cycle of atmospheric moisture.
86 In addition, most studies have focused on UTH (a vertically-weighted integral of relative
87 humidity zooming in the upper troposphere) rather than considering the vertical distribution
88 of humidity. Moradi et al. (2016) showed that peak times for tropospheric relative humidity
89 varied throughout the tropical belt using the Megha-Tropiques satellite. Chepfer et al.
90 (2019) used the CATS spaceborne lidar to related this diurnal variability to the vertical
91 properties of clouds.

92 In this study we analyze the relationships between clouds and atmospheric relative hu-
93 midity (RH) and their joint diurnal variations by fully exploiting an ensemble of observation
94 data from different space-borne instruments. We address the following question:

95 How are RH and clouds linked at the sub-daily scale ? Specifically is there a signature
96 in RH before or after the cloud growth at the sub-daily scale ?

97 We focus on the tropical Western Atlantic region, (70°W - 30°W in latitude and 10°N -
98 30°N in longitude) subjected to the large-scale forcing of the downward branch of the Hadley
99 cells. This region is mostly characterized by shallow convection and most clouds are Stra-
100 tocumulus and Cumulus. Vial et al. (2019) discussed the diurnal variability of cloud-base in
101 this region through the prism of ground-based measurements and regional models. We aim
102 to expand previous studies that investigated the diurnal variations of the ITCZ (Ruppert
103 & Johnson, 2015; Ciesielski et al., 2018; Sakaeda et al., 2018) at its edges and offer new
104 insights on the diurnal cycle of the subsiding branch of the overturning circulation.

2 Data and Methods

2.1 Datasets

Satellite estimates of cloud types and RH profiles are combined with other environmental parameters from the European Center for Medium-range Weather Forecast (ECMWF) ERA-5 reanalysis (Hoffmann et al., 2019).

The RH profiles are derived from the SAPHIR sounder on Megha-Tropiques. Since October 2011, this satellite provides 3 to 5 observations daily at any given point of the tropics. Its equatorial crossing time shifts backward by 100min due to the precession cycle of the platform (Roca et al., 2015). SAPHIR provides humidity profiles throughout the troposphere by sampling the atmospheric moisture in the 183.31 GHz line with six channels. The 1700km-swath of SAPHIR covers the $\pm 30^\circ$ equatorial belt. Its nominal observations are performed at a horizontal resolution of 10km at nadir. Here we use the operational Level 2 RH profiles described in Sivira et al. (2015) and Brogniez et al. (2016). RH is preferred over absolute humidity to avoid dependency to temperature profiles.

Cloud types are taken from the Numerical Weather Prediction - Satellite Application Facility (NWP-SAF) algorithm developed for geostationary satellites (Derrien & Le Gléau, 2005; Sèze et al., 2015). A finer spatial scale is available for these cloud types than for RH profiles, which provides up to 20 geostationary pixels within each of the larger SAPHIR footprints. We consider five cloud types: "Very Low" with cloud top pressure $P_{top} > 800\text{hPa}$, "Low" with $P_{top} \in [650\text{hPa}; 800\text{hPa}]$, "Medium" with $P_{top} \in [450\text{hPa}; 650\text{hPa}]$, "High Opaque" and "High Semi-transparent" with $P_{top} < 450\text{ hPa}$. Among the cloud types in the trade winds, as defined by (Riehl, 1954), the Very Low category can be associated with shallow convective clouds with tops that do not exceed 4km, such as Cumulus Humilis and Chimney clouds. High Opaque and High Semi-transparent clouds are distinguished from each other by their concentration of water (ice/liquid) and their optical thickness.

The conditional evolution of RH for a given cloud type is nailed down by selecting SAPHIR footprints dominated by a given cloud type : if more than 90% of a SAPHIR footprint is filled with geostationary pixels of the same type, then the corresponding RH profile is attributed in its entirety to this particular type. This cautious selection retains only $\sim 30\%$ of the total observations. It allows to extract clear co-variations between the clouds and the corresponding RH profiles.

136 Environmental conditions are described with ECMWF ERA-5 outputs at the 0.75°
 137 latitude-longitude resolution grid:

- 138 1. skin temperature (SkT), used to relate to the solar heating;
- 139 2. air temperatures at 500hPa (T_{500}) and 200hPa (T_{200}), to deconstruct the moisture
 140 and temperature signatures within the variability of RH;
- 141 3. lower tropospheric stability (LTS) that provides a measure of the inversion strength
 142 between the surface (θ_0) and above the atmospheric boundary layer (ABL) at 700hPa
 143 (θ_{700}) (Klein & Hartmann, 1993);
- 144 4. 10-m wind divergence ($\nabla \vec{U}_{10m}$) and 500hPa-vertical atmospheric velocity (ω_{500}) as
 145 indicative of the dynamical flows.

146 All these parameters are considered at the hourly time scale, except ω_{500} that is used at the
 147 monthly time scale to define climatologically stable conditions. All outputs are translated
 148 into the local time of observation (LT).

149 2.2 Method: composite diurnal cycle

150 All instantaneous observations from the Western Atlantic sub-region taken during the
 151 periods January-February-March (JFM) and July-August-September (JAS) 2012-2017 are
 152 gathered to create a composite diurnal cycle for all variables.

153 In order to link with large-scale dynamics, the data is categorized into ascending ($\omega_{500} < 0$)
 154 and subsiding ($\omega_{500} > 0$) categories. Relative anomalies of each variable with respect to
 155 their daily averages are computed as follows:

$$156 \quad Y'(t) = 100 \times \frac{Y(t) - \bar{Y}}{\bar{Y}} \quad (1)$$

157 where $Y(t)$ is either the number of situations of a given cloud type or the RH value at a
 158 given pressure level at time t (hours), and \bar{Y} is the corresponding daily mean.

159 Harmonic functions are fitted on the composite hourly time series using a least-squared error
 160 method, with a diurnal harmonic (24h cycle) and a semidiurnal harmonic (12h cycle; see
 161 example on Fig. 3). From these fits, lagged-correlations are computed between anomalies
 162 of RH with respect to time t and X (cloud prevalence or environmental parameters) with
 163 respect to time $t + i$. They are noted $R(i)$ for a time lag i , with σ_{RH} and σ_X the variances
 164 of RH and X :

$$165 \quad R(i) = \frac{E[(X_t - \bar{X})(RH_{t+i} - \bar{RH})]}{\sigma_X \sigma_{RH}} \quad (2)$$

166 The correlation significance is tested with a Student t-test (95% confidence interval).

167 **3 Results**

168 **3.1 Regional temporal variability**

169 Figure 1 displays the seasonal differences in large-scale circulation in the tropical West-
 170 ern Atlantic area with a climatology of ω_{500} (Fig.1 a-b) and the diurnal fluctuations of SkT,
 171 ∇U_{10m} and LTS (Fig.1 c-d). During JFM, this region is subjected to strong subsidence
 172 aloft (Fig.1 a). During JAS, the region is on the edge of the ITCZ and is generally charac-
 173 terized by weaker vertical motions (Fig.1 (b)). In terms of cloudiness, the two seasons are
 174 populated by different cloud types: during the JFM period, low-altitude clouds associated
 175 with the trade winds are dominant, while the JAS period is characterized by both high and
 176 low-altitude clouds associated with the ITCZ ((Konsta et al., 2012); see also Fig. 2). We
 177 focus on the large-scale subsiding category ($\omega_{500} > 0$) to minimize the sampling of deep
 178 convective systems by the SAPHIR microwave sounder (Burns et al., 1997; Brogniez et al.,
 179 2013).

180
 181 The environmental conditions displayed on Figures 1c-d provide insight into the pro-
 182 cesses governing the formation of clouds. Surface warming by solar heating reaches a maxi-
 183 mum at 12:00 LT, and is associated with a known weak cycle in $\nabla \vec{U}_{10m}$ (Nitta & Esbensen,
 184 1974), that is almost inexistent during JAS, and with a steadily increasing LTS. The diurnal
 185 variations in LTS indicate lower instability in the morning hours (minimum of LTS at 4:00
 186 LT) at the same time as the peak of cloud occurrences (Fig. 2 a-e). In both seasons, in-
 187 creased stability is observed as the day progresses until a peak is reached around 18:00-20:00
 188 LT which inhibits vertical cloud extension. In JFM, a second peak of LTS is observed at 9:00
 189 LT coinciding with the start of solar heating, and, to a lesser extent, with the daily maxi-
 190 mum of wind convergence. Vertical heating of the atmosphere shifts progressively over time
 191 from the bottom (SkT, maximum at 12:00 LT) to the middle (T_{500} , maximum at 16:00 LT)
 192 and then to the top (T_{200} , maximum at 20:00 LT, with a second maximum near 8:00-10:00
 193 LT).

194 Figure 2 shows the hourly evolution of the prevalence of the five cloud types within
 195 the Western Atlantic area along with the daily fluctuations in the average RH profile for
 196 JFM (a-d) and JAS (e-h). In order to highlight the amplitude of the diurnal cycle, relative

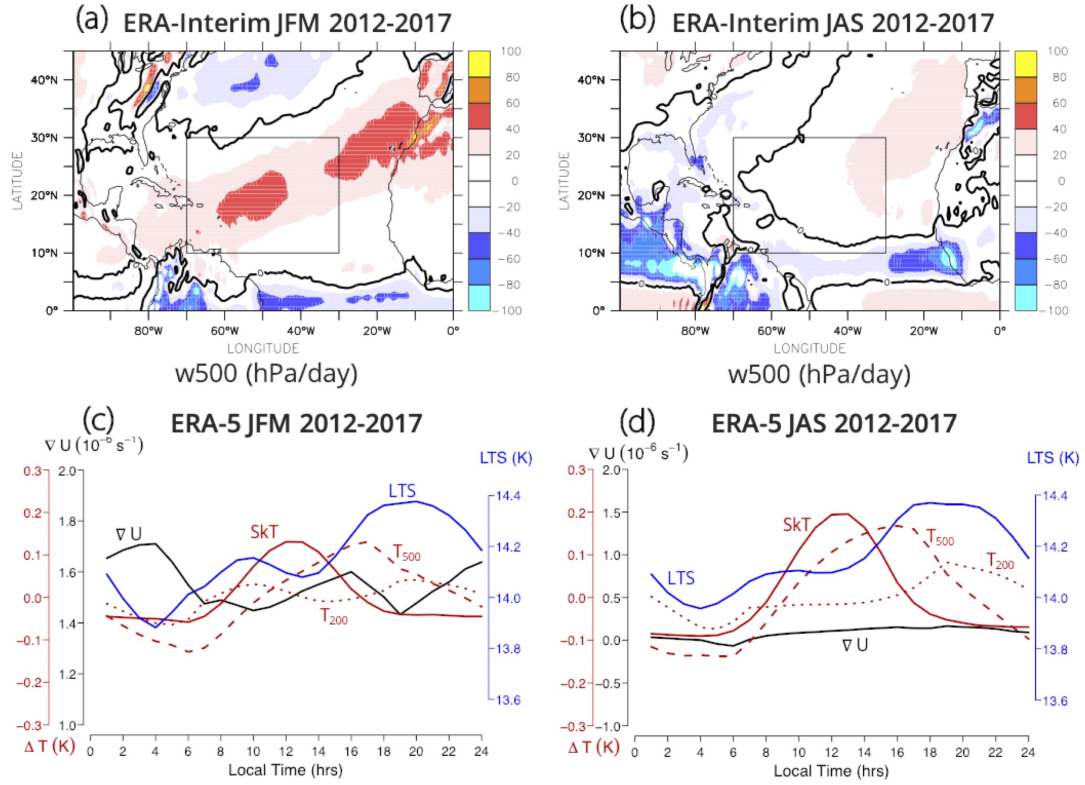


Figure 1. (top panel) Interannual averages of the 500hPa atmospheric vertical velocity (hPa/day) computed over the period 2012-2017 for (a) JFM and (b) JAS. The isoline indicates $\omega_{500} = 0$ hPa/day. The box delineates the area of interest. (bottom panel) Composite diurnal cycles for (c) JFM and (d) JAS defined for the area of interest indicating: the average divergence for the 10-m wind (∇U in 10^{-6} s^{-1} ; black curve), anomalies of SkT (in K; red curve), T_{500} (in K; red-dashed curve) and T_{200} (in K; red-dotted curve), and the average LTS (in K; blue curve).

197 anomalies with respect to the mean daily states are shown by cloud types (Fig. 2 b and f)
198 and for RH (Fig. 2 c and g). Figures 2 (d) and (h) present the daily variations of RH in
199 situations filled with "Very Low" clouds exclusively.

200 Figures 2 (a) and (e) confirm that the VeryLow clouds are the dominant cloud type dur-
201 ing JFM, followed by HighSemi clouds. The contributions of VeryLow, Low and HighSemi
202 are more evenly prevalent during JAS. During both periods the frequency of occurrence of
203 these cloud types indicate a strong diurnal cycle with a peak around 7:00 LT, and a dip
204 early afternoon around 13:00 LT, as the solar heating inhibits the vertical development of
205 clouds by stabilizing the column (Randall et al., 1991).

206 During both seasons, total cloud distribution for the VeryLow and Low classes (and to a
207 lesser extent Medium) reaches a peak in the morning, between 0:00 LT and 8:00 LT caused
208 by shallow convection (Fig. 2b-f). While VeryLow clouds display similar diurnal variations
209 across both seasons, there are seasonal variations in the diurnal cycles of the other cloud
210 types. The peak of the diurnal cycle for Low clouds shifts from 6:00-8:00 LT in JFM to
211 0:00-2:00 LT in JAS, and for HighOpaque and HighSemi clouds it shifts from the morning
212 (4:00-11:00 LT) in JFM to the afternoon (12:00-20:00 LT) in JAS. The higher the clouds,
213 the greater the shift in peak occurrence between JFM and JAS.

214 During the JAS period, HighOpaque cloudiness is maximal in the late afternoon and
215 early night (16:00-24:00 LT). It coincides with a moistening of the upper troposphere (Fig.
216 2 b). This moistening may be induced by their detrainment of moisture (Soden & Fu, 1995;
217 Sassi et al., 2001; Garot et al., 2017) and by local lifting of moisture in regions of high cloud
218 cover.

219 The diurnal variations of the tropospheric RH are shown in Fig 2 (c) and (g). The
220 vertical profile displays diurnal vertical heterogeneity. The relative variations of RH within
221 the ABL (~ 850 -950 hPa) are of lower amplitude than in other layers. This is normal because
222 the ocean surface maintains moist conditions in the ABL all day-long ($\sim 80\%$) and lessens
223 moisture variations. In this layer, RH peaks around 6:00-8:00 LT when the cloud cover is
224 maximal. Just above (~ 800 -600 hPa), RH diurnal variations are maximal around 4:00 LT.
225 A weak secondary moistening is visible around 20:00 LT in JFM. In the free troposphere
226 (~ 600 -300 hPa) this maximum point shifts to an earlier time (2:00-4:00 LT), and in both
227 JFM and JAS, the maximum point is reached in the evening around 20:00 LT. Finally, in
228 the upper layers (above 300 hPa) the first maximum point disappears and is replaced by a

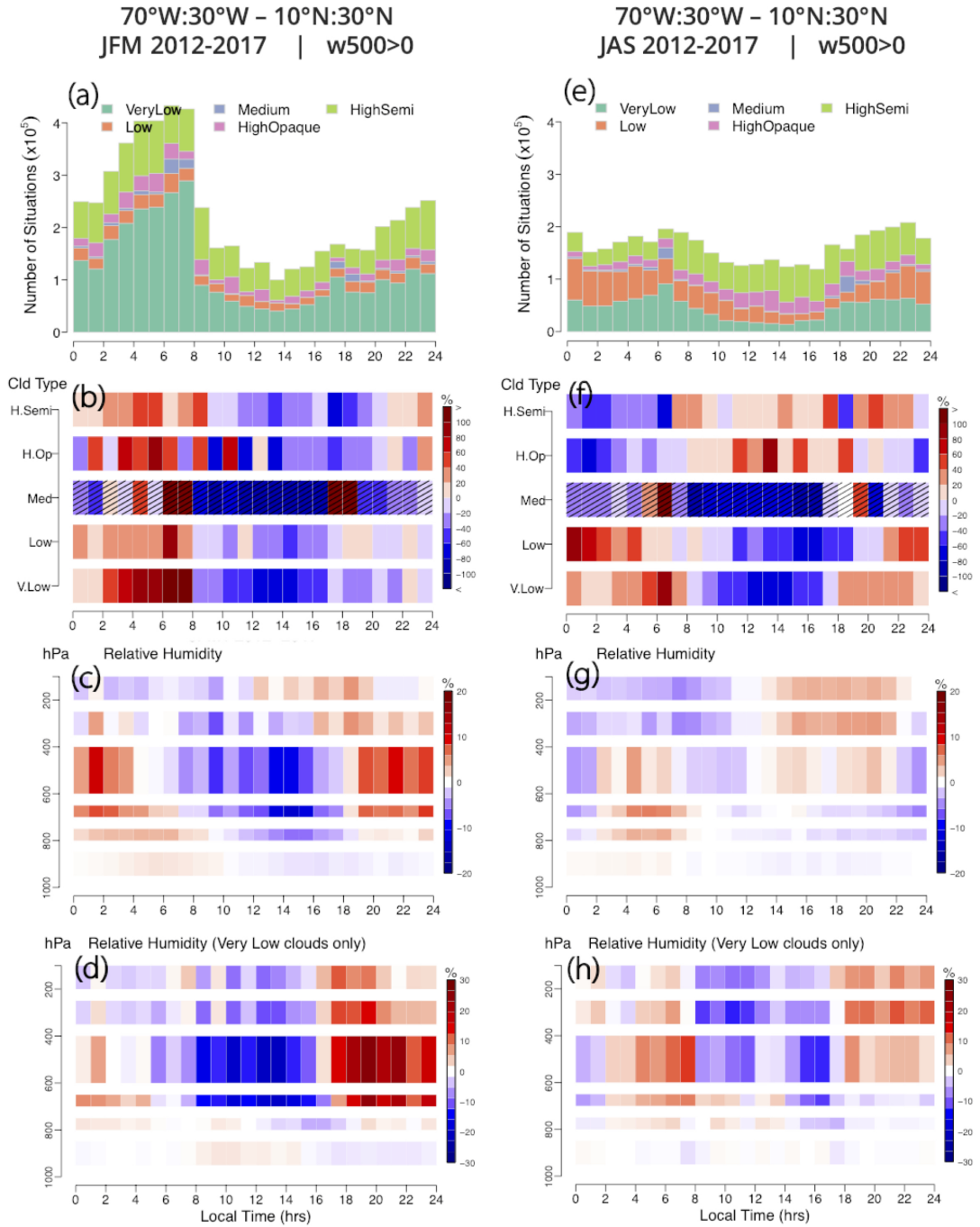


Figure 2. Composite diurnal cycles defined over the tropical Western Atlantic region during JFM (left column) and JAS (right column) over the period 2012-2017. Panels (a) and (e): prevalence of each cloud type accumulated for the area. Panels (b) and (f) : relative anomaly of cloud prevalence compared to their respective daily averages (in %). The hatched part indicates that the computation is performed with less than 1% of the total population. Panels (c) and (g) : relative anomaly of the vertical profiles of RH relative to the daily average of the considered atmospheric layer (in %). (d) and (h) same as (c-g) but using only the RH profiles associated with VeryLow clouds.

229 strong drying while afternoon moistening is strengthened. These patterns are similar overall
 230 between the two seasons, but the diurnal gradients are weaker during JAS, when the region
 231 is on the edge of the ITCZ, compared to JFM, when the region is located within a strong
 232 large-scale subsidence. Fig 2 (c) and (g) reveal a vertical consistency across layers, with
 233 the moistening and drying shifting over time from the top layers to the bottom layers. It
 234 suggests that both the large-scale subsidence and diurnal pulses in the fluxes of atmospheric
 235 moisture have an influence.

236 The variability of RH in situations where only VeryLow clouds are detected in the
 237 SAPHIR pixels is presented in Fig 2 (d) and (h). Under these conditions, the vertical
 238 diurnal cycles of RH are more similar during JFM and JAS, with a strong daytime drying
 239 of the mid-troposphere (700 to 300 hPa) surrounded by moister atmospheric layers, and an
 240 early night moistening which becomes remarkably stronger after sunset (18:00-22:00 LT)
 241 during JFM. The JAS cycle is more pronounced in this case when compared to the cycle
 242 including all cloud types (Fig. 2 (g)). This confirms that the vertical structure and diurnal
 243 variations of atmospheric moisture is strongly related with the diurnal cycle of clouds. The
 244 RH vertical diurnal cycle remains less pronounced during JAS than during JFM, which may
 245 be due to the lower frequency of prevalence of VeryLow clouds during JFM.

246 **3.2 Analysis of correlations**

247 To quantify the relationships between the moisture field and the clouds, Figure 3 dis-
 248 plays lagged correlations between the harmonic fits on the RH profiles and the number of
 249 each cloud type. We also show the lag between the maxima as well as the lag between
 250 the minima defined from the fitted hourly evolutions. While the temperature is the first-
 251 order driver of RH, the other environmental parameters are also closely linked to RH at
 252 the diurnal scale. These statistics reveal that the co-variations between the different cloud
 253 categories and RH the low troposphere on one hand, and RH in the free troposphere on the
 254 other hand, have notable opposite variations during JFM. This is less obvious for JAS.

256 **3.2.1 Winter patterns**

257 During JFM, RH diurnal variations display similar departures with respect to the Very-
 258 Low and Low diurnal variations. Below 750hPa, the diurnal variations of RH are highly

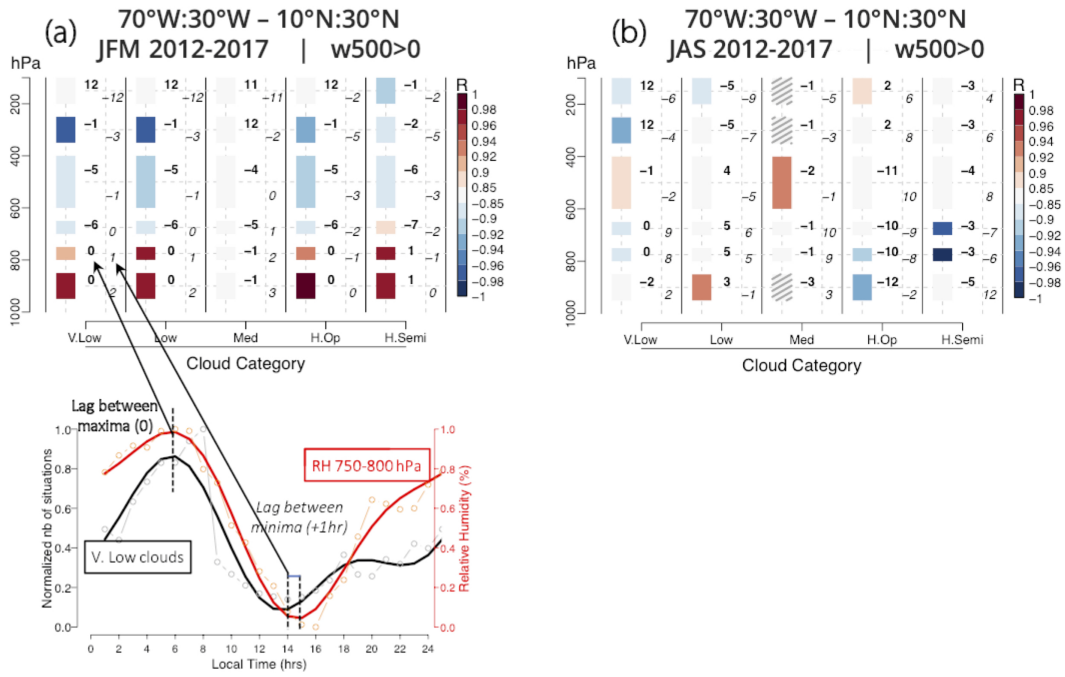


Figure 3. Lagged correlation (intensity in color scale) computed for the subsiding regime category between RH at a given pressure level and the cloud prevalence sorted by category. (a) January-February-March (JFM) and (b) July-August-September (JAS). As described by the inset below, the bold number is the lag between the maximum of the two times series and the italic number is the lag between their minimum. If the lag is <0 then the maximum/minimum of the chosen cloud prevalence precedes the maximum/minimum of RH. Dashed boxes are non-significant correlations with p .values > 0.05 .

259 correlated with those of the VeryLow ($R_{V.Low}=0.90-0.96$) and Low ($R_{Low}=0.97$) cloud cat-
 260 egories. Such correlations suggest that common processes link both diurnal cycles in the
 261 PBL. The clouds and RH maxima coincide (lag=0) while the RH diurnal minima are slightly
 262 shifted with respect to the cloud minima (1 to 2 hours). This delay is consistent with Fig.
 263 2 (b) and (c) and indicates that the moistening of the layer may result from the dilution of
 264 low-level clouds as suggested by (Eastman & Warren, 2014). Note that it coincides with the
 265 daytime increase of T_{500} (Fig. 1c), so the drying processes of this part of the atmosphere are
 266 in phase with the warming of the free troposphere. This suggests that the daytime warming
 267 of the mid-troposphere, through shortwave (near-infrared) absorption by clouds and water
 268 vapor, as well as by the surface heating, is strongly linked to the dilution of low-level clouds
 269 and the subsequent moistening of the near-surface troposphere.

270 In the mid-troposphere ($\sim 700-400\text{hPa}$) correlation magnitudes remain high but become neg-
 271 ative ($R_{V.Low}=-0.88$, $R_{Low}=-0.90$), with little to no lag between minima, while RH peaks
 272 5-6hrs earlier than the clouds. It suggests that processes different than those in the PBL
 273 jointly affect the diurnal cycles of RH and clouds. Moving to the upper troposphere, the
 274 RH diurnal minima increasing lead the cloud diurnal minima (e.g. -3 hrs at 250-350hPa),
 275 while the lead of RH diurnal maxima gradually decreases (e.g. from -5 hrs at 400-600hPa
 276 to -1 hr at 250-350hPa), indicating that the processes at play are vertically connected.

277 The correlations and lags profiles of the RH diurnal variations display similar features with
 278 HighOpaque and HighSemi clouds. As for VeryLow and Low clouds, in the PBL the corre-
 279 lations are high and positive while somewhat lower and negative in the mid-troposphere.

280 The RH diurnal minima increasing lead the cloud diurnal minima from the surface (lag=0hr)
 281 to 250-350hPa (lag=-5hrs) except at the highest altitude range (lag=-2hrs). The RH max-
 282 ima display slight or no delay in the PBL, and significant leading time just above the PBL
 283 (lag $\sim -6\text{hrs}$) that decreases with altitude. As noted in Fig 2 (c) and (g), the moistening
 284 and drying shifts over time from the top layers to the bottom layers suggest the influence
 285 of large-scale subsidence and diurnal pulses in the fluxes of atmospheric moisture.

286 It is hypothesized that the warming of the mid-troposphere by shortwave absorption
 287 triggers air masses to lift a few hours later from increased buoyancy produced by heating
 288 (Ackerman et al., 1988; Mather et al., 2007; Powell et al., 2012). This lifting causes the mid-
 289 troposphere to dry while supplying the upper tropospheric layer with additional moisture.
 290 This moisture is later pumped to maintain HighSemi clouds that could develop from the
 291 debris of dissipating HighOpaque clouds (i.e. anvils) (Luo & Rossow, 2004). Such physical

292 links could be evaluated in hourly reanalyses such as ERA5, by looking at the similarities in
293 the diurnal cycles of clouds and RH and at the evolution of the 3-D wind field and heating
294 profiles. The use of field campaigns data (e.g. the recent EUREC4A campaign; Bony et al.
295 (2017)) would also be greatly beneficial.

297 *3.2.2 Summer patterns*

298 During JAS, large-scale ascent associated with the ITCZ influences the cloud processes
299 in the region. The observed diurnal moisture and clouds variabilities are more strongly
300 associated with the diurnal pulses of the ITCZ than during JFM. The higher diversity of
301 cloud types in JFM (Fig. 2e) makes it more difficult to analyze how a specific cloud type
302 affects the RH diurnal cycle. It is reflected by the lower correlations between RH diurnal
303 variations and those of clouds than during JFM. For example, the correlations with the
304 Medium cloud category is weak or non-significant.

305 The profiles of correlation and lags display less structure than during JFM, but one can
306 note specific patterns. First, the lags between the maxima of RH and clouds prevalence
307 change their sign near 400hPa for all clouds categories but HighSemi. This suggests that
308 different moistening processes occur below and above 400hPa. In situations of HighSemi
309 cloud cover the entire troposphere moistens 3 to 5 hrs after the cloud maximum growth.
310 Second, the lags between the minima change their sign near 700hPa for all cloud categories
311 without exception. Hence, a drying below 700hPa precedes the minimum of formation for
312 the VeryLow and Low clouds while above this is the opposite (minimum of clouds before
313 minimum of RH). For the HighOpaque and HighSemi clouds, the processes at play turn
314 the diurnal cycles: below 700hPa the minimum of RH follows the minimum of prevalence
315 of these clouds (6 to 9 hrs after) while above the drying precede their dissipation by 4 to
316 10hrs.

317 We believe that these results corroborate studies on the diurnal variabilities of convection
318 and precipitation that highlight radiative-dynamics-convective interplays (Randall et al.,
319 1991). These studies suggest that large anvil clouds dampen the heating of the atmospheric
320 column (via their shade). It feedbacks on precipitation via locally-enhanced upward motion
321 within the cloudy column as compared to neighboring cloud-free columns (Chen & Houze,
322 1997; Ruppert & Klocke, 2019).

323 The moistening patterns of the upper troposphere observed during the JFM period
 324 point towards different mechanisms. Overall the presence of upper level cloudiness is sig-
 325 nificantly reduced. Peak occurrence (albeit small) is observed near sunrise while there is
 326 an upper level moistening between 14:00 and 22:00 LT. This local moistening is more pro-
 327 nounced when no elevated clouds are present in the column (Fig. 2 (d)). It could be induced
 328 by horizontal advection of moisture from remote areas (Pierrehumbert & Roca, 1998; Sher-
 329 wood et al., 2010), and could be associated to the diurnal pulses of the ITCZ (Ciesielski et
 330 al., 2018) as well as by variations in the upward motion forced by solar heating.

331 **4 Summary and conclusions**

332 In this study, we show how the Megha-Tropiques satellite adds value to the study of
 333 the diurnal cycle of atmospheric moisture. By collocating SAPHIR observations with those
 334 of cloud types and environmental conditions over the Western Atlantic Trades during JFM
 335 and JAS 2012-2017, a robust depiction of the diurnal co-evolution of clouds and moisture
 336 in areas remotely connected to the rainy ITCZ is provided.

337 Here, we target the diurnal variation of RH in areas less affected by strong convective
 338 motions and dominated by a mean downward flow. Fig. 4 provides a sketch that summarizes
 339 the observed patterns.

340 In the strongly subsiding situation ($\omega_{500} \gg 0$, corresponding to JFM) :

- 341 (i) After sunrise (06:00-12:00 LT), the mid-troposphere is mostly free of clouds and under-
 342 goes a strong drying linked to the mean downward motion that brings dry air masses from
 343 the colder upper troposphere.
- 344 (ii) The daytime warming (12:00-18:00 LT) of the mid-troposphere is linked to the dilution
 345 of low-level clouds and triggers moistening of the low troposphere a few hours later.
- 346 (iii) At sunset (18:00-24:00 LT), the longwave radiative cooling starts to dominate, thereby
 347 increasing the vertical cooling rate. The increased temperature gradient yields mixing mois-
 348 ture vertically. We hypothesize that this behavior is remotely connected to the ITCZ diurnal
 349 pulses and its afternoon peak, as suggested by (Ruppert & Klocke, 2019).
- 350 (iv) The lifting of moist air in the upper troposphere triggers the formation of high-altitude
 351 cirriform clouds at night (18:00-24:00 LT). Moisture is pumped from below to maintain
 352 them.

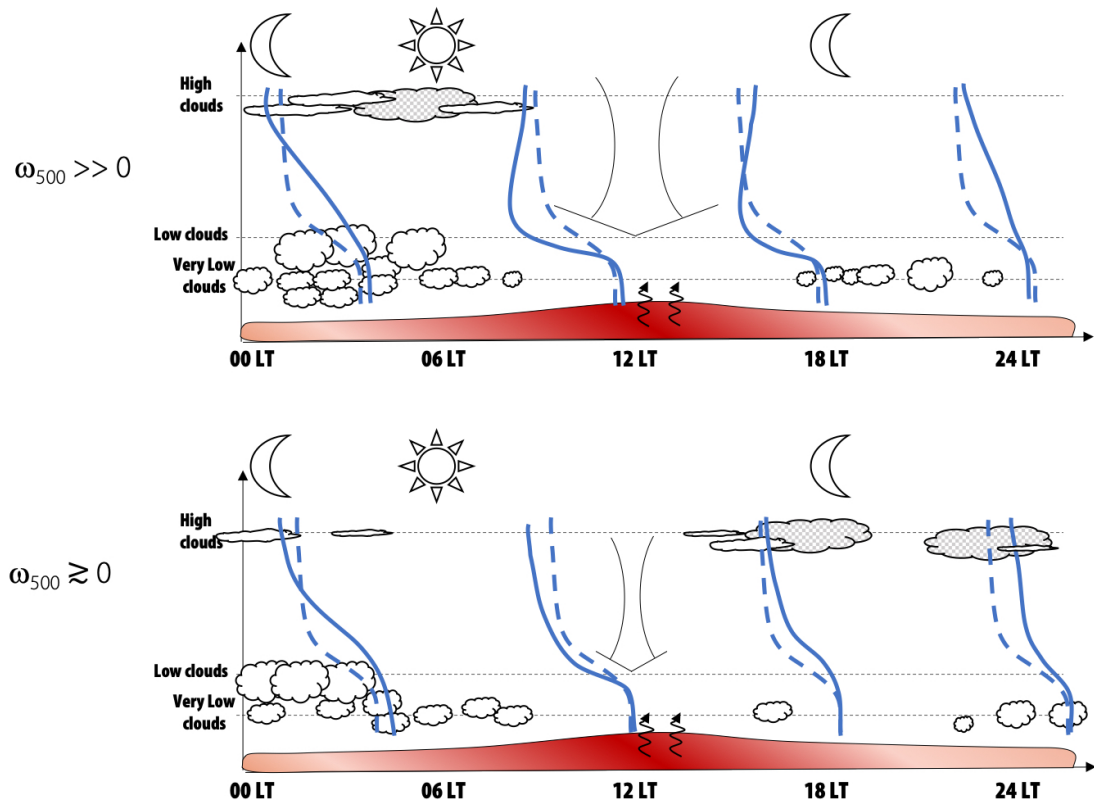


Figure 4. Diagram that shows the evolution of the RH profile (solid line) around its daily average (dashed line). The top panel is for the period of strong subsidence (i.e. JFM, $\omega_{500} \gg 0$) and the bottom panel is for the period of moderate subsidence (i.e. JAS, $\omega_{500} \approx 0$). HighOpaque clouds are in gray while HighSemi clouds are in white, and the large vertical arrows represent the mean downward motions.

353 In the moderate subsiding situation ($\omega_{500} \simeq 0$, corresponding to JAS) :

354 (i) The presence of high-altitude clouds during daytime (12:00-18:00 LT) shields the atmo-
355 spheric column from solar forcing and reduces the drying due to large-scale subsidence.

356 (ii) The development of upper tropospheric opaque clouds after sunset (18:00-06:00 LT),
357 associated with the ITCZ convective systems, constitutes a local source of moisture via
358 detrainment.

359 It is hypothesized that the development of VeryLow and Low clouds is driven by con-
360 ditions independent of the season, whilst the other categories of clouds are driven by large
361 scale dynamics conditioned by the seasonal variations of the ITCZ.

362 These findings help to refine an atmospheric moisture budget for a quiescent area of the
363 tropics, and emphasize the important role of relative humidity constrained by clouds and
364 dynamics. In future works the impact of the seasonal and diurnal variability of the ITCZ
365 will be considered thanks to this observational dataset. The impact of these connections
366 will be explored by taking the entire tropical belt into consideration, and by looking at
367 moisture profiles dependent on cloud types. This undertaking will contribute to improve
368 the assessment of the cloud-water vapor feedback.

369 **Acknowledgments**

370 H. B. acknowledges CNES for its financial support for the scientific activities within the
371 Megha-Tropiques project. P.-E. K. acknowledges funding through the Labex IPSL program.
372 We also thank J. Ruppert for fruitful exchanges on the diurnal feedbacks and Mary Minnock
373 for her English revision. We also thank the reviewers for their suggestions and comments
374 that helped to improve the manuscript. The support of S. Bouffiès-Cloch e on ERA5 data
375 is greatly appreciated, as is that of the IPSL/ESPRI for providing computing resources.
376 We also thank the national Aeris data center that hosts the entire Megha-Tropiques data
377 archive. All data used are freely available from the Aeris portal <https://en.aeris-data.fr>.

378 **References**

- 379 Ackerman, T., Liou, K.-N., Valero, F., & Pfister, L. (1988). Heating rates
380 in tropical anvils. *J. Atmos. Sci.*, *45*(10), 1606-1623, doi:10.1175/1520-
381 0469(1988)045<1606:HRITA>2.0.CO;2.
- 382 Bellenger, H., Takayabu, Y. N., T., U., & K., Y. (2010). Role of diurnal warm layers in

- 383 the diurnal cycle of convection over the tropical Indian Ocean during MISMO. *Mon.*
384 *Wea. Rev.*, *138*, 2426-2433, doi:10.1175/2010MWR3249.1.
- 385 Bony, S., Stevens, B., Ament, F., Bigorre, S., Chazette, P., Crewell, S., . . . Wirth, M. (2017).
386 EUREC4A: a field campaign to elucidate the Couplings between clouds, convection
387 and circulation. *Surv. Geophys.*, *38*, 1529-1568, doi:10.1007/s10712-017-9428-0.
- 388 Bony, S., Stevens, B., Frierson, D. M., Jakob, C., Kageyama, M., Pincus, R., . . . Webb,
389 M. J. (2015). Clouds, circulation and climate sensitivity. *Nature Geosci.*, *8*, 261-268,
390 doi:10.1038/ngeo2398.
- 391 Brogniez, H., Fallourd, R., Mallet, C., Sivira, S., & Dufour, C. (2016). Estimating con-
392 fidence intervals around relative humidity profiles from satellite observations: ap-
393 plication to the SAPHIR sounder. *J. Atmos. Oceanic Technol.*, *33*, 1005-1022,
394 doi:10.1175/JTECH-D-15-0237.1.
- 395 Brogniez, H., Kirstetter, P.-E., & Eymard, L. (2013). Expected improvements in the
396 atmospheric humidity profile retrieval using the Megha-Tropiques microwave payload.
397 *Q. J. R. Meteorol. Soc.*, *139*, 842-851, doi:10.1002/qj.1869.
- 398 Burns, B., Wu, X., & Diak, G. (1997). Effects of precipitation and cloud ice on brightness
399 temperatures in AMSU moisture channels. *IEEE Trans. Geosci. Remote Sens.*, *35*,
400 1429-1437.
- 401 Chen, S., & Houze, R. (1997). Diurnal variation and life-cycle of deep convective sys-
402 tems over the tropical Pacific warm pool. *Q. J. R. Meteorol. Soc.*, *123*, 357-388,
403 doi:10.1002/qj.49712353806.
- 404 Chepfer, H., Brogniez, H., & Noel, V. (2019). Diurnal variations of cloud and relative
405 humidity profiles across the tropics. *Nature Sci. Rep.*, *9*, 16045, doi:10.1038/s41598-
406 019-52437-6.
- 407 Chung, E.-S., Soden, B., Sohn, B.-J., & Schmetz, J. (2013). An assessment of the diurnal
408 variation of upper tropospheric humidity in reanalysis data sets. *J. Geophys. Res.*,
409 *118*, 3425-3430, doi:10.1002/jgrd.50345.
- 410 Chung, E.-S., Sohn, B.-J., Schmetz, J., & Koenig, M. (2007). Diurnal variation of upper
411 tropospheric humidity and its relations to convective activities over tropical Africa.
412 *Atmos. Chems. Phys.*, *7*, 351-381.
- 413 Ciesielski, P., Johnson, R., Schubert, W., & Ruppert, J. (2018). Diurnal cycle of the ITCZ
414 in DYNAMO. *J. Clim.*, *31*, 4543-4562, doi: 10.1175/JCLI-D-17-0670.1.
- 415 Derrien, M., & Le Gléau, H. (2005). MSG/SEVIRI cloud mask and type from SAFNWC.

- 416 *Int. J. Remote Sens.*, *26*(21), 4707-4732, doi:10.1080/01431160500166128.
- 417 Eastman, R., & Warren, S. G. (2014). Diurnal cycles of Cumulus, Cumulonimbus, Stratus,
418 Stratocumulus, and Fog from surface observations over land and ocean. *J. Clim.*, *27*,
419 2386-2404, doi:10.1175/JCLI-D-13-00352.1.
- 420 Garot, T., Brogniez, H., Fallourd, R., & Viltard, N. (2017). Evolution of the distribu-
421 tion of upper tropospheric humidity over the Indian Ocean: connection with large-
422 scale advection and local cloudiness. *J. Appl. Meteor. Climatol.*, *56*, 2035-2052, doi:
423 10.1175/JAMC-D-16-0193.1.
- 424 Hartmann, D., Hendon, H., & Houze, R. (1984). Some implications of the mesoscale
425 circulation in tropical cloud clusters for large-scale dynamics and climate. *J. Atmos.*
426 *Sci.*, *41*(1), 113-121, doi:10.1175/1520-0469(1984)041<0113:SIOTMC>2.0.CO;2.
- 427 Hoffmann, L., Gunther, G., Li, D., Stein, O., Wu, X., Griessbach, S., ... Wright, J. (2019).
428 From ERA-Interim to ERA5: considerable impact of ECMWF's next generation re-
429 analysis on Lagrangian transport simulations. *Atmos. Chem. Phys.*, *19*, 3097-3124,
430 doi: 10.5194/acp-19-3097-2019.
- 431 Klein, S., & Hartmann, D. (1993). The seasonal cycle of low stratiform clouds. *J. Clim.*,
432 *6*, 1587-1606.
- 433 Klein, S., Hartmann, D., & Norris, J. (1995). On the relationships among low-cloud struc-
434 ture, sea surface temperature and atmospheric circulation in the summertime North-
435 east Pacific. *J. Clim.*, *8*, 1140-1155.
- 436 Konsta, D., Chepfer, H., & Dufresne, J.-L. (2012). A process oriented characterization of
437 tropical oceanic clouds for climate model evaluation, based on a statistical analysis
438 of daytime A-train observations. *Clim. Dyn.*, *39*, 2091-2108, doi:10.1007/s00382-012-
439 1533-7.
- 440 Luo, Z., & Rossow, W. (2004). Characterizing tropical cirrus life cycle, evolution and
441 interaction with upper-tropospheric water vapor using Lagrangian trajectory analysis
442 of satellite observations. *J. Clim.*, *17*, 4541-4563, doi:10.1175/3222.1.
- 443 Mapes, B. E., & Houze, R. A. (1993). Cloud clusters and superclusters over the oceanic
444 warm pool. *Mon. Wea. Rev.*, *121*, 1398-1415.
- 445 Mather, J., McFarlane, S., Miller, M., & Johnson, K. (2007). Cloud properties and associated
446 radiative heating rates in the tropical western Pacific. *J. Geophys. Res.*, *112*(D05201),
447 doi:10.1029/2006JD007555.
- 448 Moradi, I., Arkin, P., Ferraro, R., Eriksson, P., & Fetzer, E. (2016). Diurnal variation of

- 449 tropospheric relative humidity in tropical regions. *Atmos. Chem. Phys.*, *16*, 6913-6929,
450 doi:10.5194/acp-16-6913-2016.
- 451 Nitta, T., & Esbensen, S. (1974). Diurnal variations in the Western Atlantic Trades during
452 the BOMEX. *J. Roy. Meteorol. Japan*, *52*(2), 254-257.
- 453 Noel, V., Chepfer, H., Chiriaco, M., & Yorks, J. (2018). The diurnal cycle of cloud profiles
454 over land and ocean between 51°S and 51°N, seen by the CATS spaceborne lidar from
455 the International Space Station. *Atmos. Chem. Phys.*, 9457-9473, doi:10.5194/acp-18-
456 9457-2018.
- 457 Pierrehumbert, R., & Roca, R. (1998). Evidence for control of Atlantic subtropical humidity
458 by large-scale advection. *Geophys. Res. Lett.*, *25*, 4537-4540.
- 459 Powell, S., Houze, R., Kumar, A., & McFarlane, S. (2012). Comparison of simulated
460 and observed continental tropical anvil clouds and their radiative heating profiles. *J.*
461 *Atmos. Sci.*, *69*, 2662-2681, doi:10.1175/JAS-D-11-0251.1.
- 462 Randall, D., Harshvardhan, & Dazlich, D. (1991). Diurnal variability of the hydrologic cycle
463 in a general circulation model. *J. Atmos. Sci.*, *48*(1), 40-62.
- 464 Riehl, H. (1954). *Tropical meteorology*. McGraw Hill, New York.
- 465 Roca, R., Brogniez, H., Chambon, P., Chomette, O., Cloché, S., Gosset, M., ... Viltard,
466 N. (2015). The Megha-Tropiques Mission: a review after three years in orbit. *Front.*
467 *Earth Sci.*, *3*, doi:10.3389/feart.2015.00017.
- 468 Rozendaal, M., Leovy, C., & Klein, S. (1995). An observational study of diurnal variations
469 of marine stratiform clouds. *J. Clim.*, *8*, 1795-1809.
- 470 Ruppert, J. H. (2016). Diurnal timescale feedbacks in the tropical cumulus regime. *J. Adv.*
471 *Model. Earth. Syst.*, *8*, 1483-1500, doi:10.1002/2016MS000713.
- 472 Ruppert, J. H., & Johnson, R. H. (2015). Diurnally modulated cumulus moistening in the
473 preonset stage of the Madden-Julian oscillation during DYNAMO. *J. Atmos. Sci.*, *72*,
474 1622-1647, doi:10.1175/JAS-D-14-0218.1.
- 475 Ruppert, J. H., & Klocke, D. (2019). The two diurnal modes of tropical upward motion.
476 *Geophys. Res. Lett.*, *46*, doi:10.1029/2018GL081806.
- 477 Sakaeda, N., Powell, S. W., Dias, J., & Kiladis, G. N. (2018). The diurnal variability
478 of precipitating cloud populations during DYNAMO. *J. Atmos. Sci.*, *75*, 1307-1326,
479 doi:10.1175/JAS-D-17-0312.1.
- 480 Sakazaki, T., Hamilton, K., Zhang, C., & Wang, Y. (2017). Is there a stratospheric pace-
481 maker controlling the daily cycle of tropical rainfall? *Geophys. Res. Lett.*, *44*, 1998-

- 482 2006, doi:10.1002/2017GL072549.
- 483 Sassi, F., Salby, M., & Read, W. (2001). Relationship between upper tropospheric humidity
484 and deep convection. *J. Geophys. Res.*, *106*(D15), 17,133-17,146.
- 485 Sèze, G., Pelon, J., Derrien, M., Le Gléau, H., & Six, B. (2015). Evaluation against
486 CALIPSO lidar observations of the multi-geostationary cloud cover and type dataset
487 assembled in the framework of the Megha-Tropiques mission. *Quart. J. Roy. Meteor.
488 Soc.*, *141*(688), 774-797, doi:10.1002/qj.2392.
- 489 Sherwood, S., Roca, R., Weckwerth, T., & Andronova, N. (2010). Tropospheric water vapor,
490 convection and climate. *Rev. Geophys.*, *48*, doi:10.1029/2009RG000301.
- 491 Sivira, R., Brogniez, H., Mallet, C., & Oussar, Y. (2015). A layer-averaged relative hu-
492 midity profile retrieval for microwave observations: design and results for the Megha-
493 Tropiques payload. *Atmos. Meas. Tech.*, *8*, 1055-1071.
- 494 Soden, B., & Fu, R. (1995). A satellite analysis of deep convection, upper-tropospheric
495 humidity and the greenhouse effect. *J. Clim.*, *8*, 2333-2351.
- 496 Stephens, G., Vane, D., Boain, R., Mace, G., Sassen, K., Wand, Z., . . . the CloudSat science
497 team (2002). The CloudSat mission and the A-Train: a new dimension of space-based
498 observations of clouds and precipitation. *Bull. Am. Meteor. Soc.*, *83*, 1771-1790, doi
499 10.1175/BAMS-83-12-1771.
- 500 Vial, J., Vogel, R., Bony, S., Stevens, B., Winker, D., Cai, X., . . . Brogniez, H. (2019).
501 A new look at the daily cycle of tradewind cumuli. *J. Adv. Model. Earth. Syst.*, *11*,
502 3148-3166, doi:10.1029/2019MS001746.
- 503 Wood, R. (2012). Stratocumulus clouds. *Mon. Wea. Rev.*, *140*, 2373-2423,
504 doi:10.1175/MWR-D-11-00121.1.
- 505 Woolnough, S., Slingo, J., & Hoskins, B. (2004). The diurnal cycle of convection and
506 atmospheric tides in an aquaplanet GCM. *J. Atmos. Sci.*, *61*, 2559-2573.
- 507 Yang, G.-Y., & Slingo, J. (2001). The diurnal cycle in the tropics. *Mon. Wea. Rev.*, *129*,
508 784-801.